Renewable Energy 212 (2023) 70–81

Contents lists available at ScienceDirect

Renewable Energy

journal homepage: www.elsevier.com/locate/renene

Rotor imbalance detection and diagnosis in floating wind turbines by means of drivetrain condition monitoring

Felix C. Mehlan *, Amir R. Nejad

Norwegian University of Technology and Science (NTNU), Jonsvannsveien 82, Trondheim, 7030, Norway

ARTICLE INFO

Keywords:
Offshore wind turbine
Rotor imbalance diagnosis
Pitch misalignment
Yaw misalignment
Mass imbalance
Drivetrain condition monitoring

ABSTRACT

This paper presents a novel approach for detection and diagnosis of the rotor imbalance types pitch misalignment, yaw misalignment and mass imbalance by monitoring the drivetrain vibration response. Traditionally, only SCADA signals including nacelle accelerations, rotor speed and electrical power are utilized for this purpose, while drivetrain condition monitoring signals are mainly used for fault detection in gears and bearings. A diagnostic method is proposed using statistical change detection methods for fault detection, phase angle estimation for localizing the faulty blade, and physics-based decision criteria for fault classification. The proposed method is tested in a numerical case study with aeroelastic and drivetrain multi-body models of the 10 MW DTU reference wind turbine. The results suggest that drivetrain condition monitoring signals are particularly beneficial for detecting and diagnosing pitch misalignment, since this fault type uniquely induces periodic out-of-plane bending moments that excite drivetrain bending modes. Drivetrain signals improved the detection rate of a 1° pitch error from 19% to near 100% and reduced the standard error in locating the faulty blade from 71.5° to 11.2°. In addition, by using drivetrain vibration amplitudes as a decision criterion, all considered pitch error cases are correctly distinguished from other fault types.

1. Introduction

Recent market trends show an increase in offshore wind turbine installations driven by higher energy yields and fewer land displacement and noise issues compared to onshore sites [1]. However, offshore wind turbines are faced with additional reliability challenges. Replacement and repair of components is expensive and time-consuming due to difficulties accessing the site and dependency on good weather conditions. Thus, unscheduled downtimes as a result of component failure can lead to high operational and maintenance expenditures (O&M). For offshore wind turbines the O&M expenditures can reach 34% of the levelised cost of energy (LCOE) [2]. A major contributor to O&M expenditures is the rotor system consisting of blades, hub, pitch actuators and bearings with frequent failures and long downtimes [3]. Imbalances in the rotor system are considerably harmful, as they not only reduce the electrical power output [4,5], but also increase fatigue loads on the blades and the tower [6].

The term imbalance refers in this article to physical disturbances of the rotor system and is not to be confused with class imbalance, which describes the uneven distribution of training data in data-driven fault diagnosis methods. Rotor imbalances are generally categorized as aerodynamic imbalances, which include pitch and yaw misalignment, and mass imbalances. Pitch misalignment refers to the incorrect angular positioning of one or multiple blades and can be caused by manufacturing errors, installation errors or failures of pitch sensors and actuators. Certification guidelines (GL Standards, 2010, Sect. 4.3.4.1, pp. 4–20) require relatively small pitch misalignment of ±0.3° [7]. Nonetheless, a recent measurement campaign of 1100 turbines revealed that 38% of operating turbines do not meet these requirements [8]. Yaw misalignment, the misalignment of rotor axis and wind direction, occurs to a degree in most operating wind turbines, since yaw control systems activate only when the yaw angle exceeds a certain threshold in order to reduce duty cycles [9]. In addition to operational yaw misalignment, the inaccuracy of wind wanes due to wake turbulence, poor calibration or errors on the control side can cause static or dynamic misalignment. Residual mass imbalance can occur due to imperfect manufacturing and installation of the blades, which is generally alleviated before commissioning of the turbine, where the rotor is rebalanced by technicians according to ISO 21940-11:2016 [10] by adding compensating masses. During operation, however, accretion of dirt, moisture or ice can cause additional mass imbalance [11].

Research on wind turbine faults generally falls into to the areas of fault diagnosis, fault prognosis and resilient control. Fault diagnosis refers to the detection and classification of different failure modes, fault prognosis describes the prediction of the fault progression and

* Corresponding author.
E-mail address: felix.c.mehlan@ntnu.no (F.C. Mehlan).

https://doi.org/10.1016/j.renene.2023.04.102
Received 21 November 2022; Received in revised form 16 March 2023; Accepted 21 April 2023
Available online 27 April 2023

remaining useful life, and resilient control is a technique to minimize the effects of faulty components on the wind turbine operation [12]. This paper, like most publications on rotor imbalance, is exclusively concerned with fault diagnosis.

Effective techniques for rotor imbalance detection are frequency-domain methods, which monitor the once per revolution (1P) frequency peak. This is based on the knowledge that in the case of rotor imbalance faults the aerodynamic, gravitational or inertial forces are not in balance, such that the turbine is excited with additional periodic loads at the rotor frequency 1P. The SCADA signals rotor speed and side-side nacelle accelerations are the state-of-the-art for rotor imbalance detection according to Hyers et al. [13]. Studies have also demonstrated the possibility of rotor imbalance detection with electrical signatures of the generator [14,15] or by direct measurement of blade loads with strain gauges [9,11].

While rotor imbalance detection is straightforward, more research is required for diagnostics, which includes the classification of different rotor imbalance types and the estimation of the fault severity, e.g the pitch or yaw angle. Niebsch et al. [16] developed a method for simultaneous estimation of mass and aerodynamic imbalances, which entails physical modelling of rotor imbalances and wind turbine dynamics, and solving the inverse problem. Kusnick et al. [11] argue that pitch misalignment decreases the power output contrary to mass imbalance and advocate for the mean power as a simple diagnostic criterion. Investigations concerned exclusively on detection and diagnosis of pitch misalignment are found in [7,17,18]. Bertele et al. propose a method for pitch misalignment detection and correction that linearly correlates the error in pitch angle with the amplitude of nacelle accelerations at 1P [7]. Cacciola et al. as well as Cho et al. use neural networks to quantify pitch misalignment severity and identify the faulty blade [17,19]. Kusiak et al. apply data mining algorithms and predictive machine learning models to diagnose pitch misalignment [18]. Many studies are devoted to indirectly estimating the yaw angle and thus circumventing the inaccuracy of wind vanes [9,20,21]. Botasso et al. estimate yaw misalignment and wind shear by observation of blade root bending moments [9]. Choi et al. apply machine learning methods to estimate yaw misalignment from SCADA data [20]. Jing et al. estimate yaw misalignment based on the reduction in electrical power output [21].

Diagnostic methods reported in literature can be broadly classified as physics-based [7,9,16], data-driven [15,17–21] and knowledge-based approaches [11], each with their own limitations. Physics-based methods require accurate aeroelastic models, which are challenging to construct and validate without full knowledge on turbine specifications and system parameters such as stiffness values. The added uncertainty from model assumptions and simplifications invariably increases the uncertainty in diagnosis. Data-driven methods on the other hand are shown to perform with high accuracy, but the challenge lies in obtaining sufficient training data of faulty conditions. Field measurements of naturally occurring faults are generally sparse and may require additional, expensive equipment such as LIDAR [20] to determine the ground truth. Knowledge-based methods rely on theoretical and practical expertise of fault causes and effects. The main difficulties lie in the acquisition and management of domain knowledge. This paper presents a knowledge-based approach to detection and diagnosis of rotor imbalance faults, summarized as follows:

1. Knowledge-based expert system
2. Classification of pitch misalignment, yaw misalignment and mass imbalances
3. Leveraging drivetrain CMS data
4. Stochastic approach that accounts for turbulence induced variance

A knowledge-based expert system is proposed, which is comprised of heuristic ‘if-then’ decision rules. The expert system is developed on the basis of domain knowledge acquired from literature review, first principles reasoning and analysis of aeroelastic simulation results. Neither physical modelling nor training data of faulty conditions are required for the method implementation.

Secondly, the proposed diagnostic method aims at distinguishing the three types of rotor imbalances pitch misalignment, yaw misalignment and mass imbalance, while earlier works have mainly focused on one fault type or the distinction of pitch misalignment and mass imbalance.

Thirdly, the proposed method incorporates drivetrain condition monitoring system (CMS) signals, while the state-of-the-art are SCADA signals characterizing global turbine dynamics such as nacelle accelerations and rotor speed. Drivetrain CMS vibration signals can provide further insight into the dynamics of the closely coupled rotor and drivetrain systems and the impact of rotor imbalances in a holistic perspective. In addition, CMS sensors are cost-effective and available in most modern offshore wind turbines.

Lastly, the proposed method explicitly accounts for the volatility of environmental conditions and the measurement noise of sensors. Statistical methods of change detection are employed here, which are proven to be robust methods for fault detection under noise and unknown disturbances and have found application in the detection of main bearing faults in earlier works [22].

The remainder of this paper is organized as follows: Section 2 presents in detail the methodology of fault detection and diagnosis, as well as the high-fidelity simulation models to evaluate the proposed method. The following Section 3 discusses dynamic system responses to rotor imbalances both qualitatively and with simulation results; and assesses the detection and diagnostic performances against a benchmark machine learning classifier. Concluding remarks are provided in Section 4.

2. Methodology

The proposed method for rotor imbalance diagnosis based on drivetrain condition monitoring is formalized in the following sections. Simulations are conducted with high-fidelity models of the global wind turbine and the drivetrain for different rotor imbalance cases and varying environmental conditions (Section 2.1). Several simulated signals are selected to emulate SCADA and drivetrain CMS signals, and are postprocessed to extract frequency- and time-domain statistical features that are indicative of rotor imbalances (Section 2.2). Statistical methods of change detection are then applied to derive test statistics for fault detection (Section 2.3.1). Classification of the rotor imbalance type uses domain knowledge formalized as an expert system (Section 2.3.2). Identification of the faulty blade is based on maximum likelihood estimates of the phase angle (Section 2.3.3). The detection and diagnostic performance of the proposed method is evaluated on simulated sensor samples of different fault and environmental conditions against a benchmark machine learning classifier (Section 2.4).

2.1. Simulation

High-fidelity dynamic simulation models based on the DTU 10 MW reference wind turbine [23] mounted on the Nautilus semisubmersible floating platform [24] are used in this study. Selected specifications of the reference turbine are listed in Table 1. The decoupled analysis approach is employed with two separate models for simulation of the global wind turbine response and the drivetrain response, respectively. The global model is implemented in the aero-servo-elastic simulation tool OpenFAST [25]. Rotor imbalances of pitch misalignment, mass imbalance and yaw misalignment are introduced in the global model. The simulated rotor hub loads and nacelle motions in six degrees of freedom obtained from the global model are imposed as boundary conditions on the higher-fidelity drivetrain model. The drivetrain model is implemented in the multi-body simulation software SIMPACK [26], which allows for detailed analysis of internal drivetrain dynamics [27].

Table 1
DTU 10MW reference turbine specifications [23].

Wind turbine type	3 blade, upwind horizontal axis
Controller type	pitch regulated, variable speed
Drivetrain type	3 stage, medium speed
Cut-in wind speed [m/s]	4
Cut-out wind speed [m/s]	25
Rated wind speed [m/s]	11.4
Rated power [MW]	10
Rotor diameter [m]	178.3
Rotor mass [kg]	229 000
Blade mass [kg]	41 000
Hub Height [m]	119.0
Gearbox ratio [–]	1:50.039
Minimum rotor speed [rpm]	6.0
Maximum rotor speed [rpm]	9.8

Table 2
Fault cases (FC). Mass imbalances are expressed in the quality grade G of ISO 21940-11:2016 [10]. Faults are constant over the entire simulation period of 4000 s.

	h	m1	m2	m3	p1	p2	p3	y1	y2	y3
Mass [–]	0	G32	G48	G64	0	0	0	0	0	0
Pitch [deg]	0	0	0	0	1	2	3	0	0	0
Yaw [deg]	0	0	0	0	0	0	0	5	10	15

Table 3
Environmental conditions (EC) with wave height H_s, wave period T_p, wind speed U and turbulence intensity I.
Source: Adopted from Nejad et al. [28].

	EC1	EC2	EC3	EC4	EC5	EC6
H_s [m]	2.0	4.5	5.0	5.0	4.0	5.5
T_p [s]	8.0	12.0	14.0	12.0	10.0	14.0
U [m/s]	4.0	7.0	10.0	12.0	14.0	20.0
I [–]	0.26	0.19	0.16	0.15	0.14	0.12
# seeds	6	6	6	6	6	6

Several fault cases are simulated, as specified in Table 2. Three cases of pitch misalignment (p1, p2, p3), mass imbalances (m1, m2, m3) and yaw misalignment (y1, y2, y3), as well as one reference case of healthy conditions (h) are considered. The selection of realistic pitch misalignment values is based on the findings of Saathoff et al. [8], who report that pitch misalignment of 0.6°–2.0° occurred in 35.3% and higher cases of $> 2°$ occurred only in 2.6% of investigated operating wind turbines. Only positive misalignment (towards feather) and only misalignment of a single blade is considered in this study. Pitch misalignment is implemented by increasing the structural twist of one blade in the aeroelastic model.

The mass imbalance cases are expressed in the imbalance quality scale G of standard ISO 21940-11:2016 [10] in accordance to Kusnick et al. [11]. The standard recommends permissible residual imbalance levels U_{per} for different applications, rotor speeds N and weight W, expressed by Eq. (1)

$$U_{per}[\text{g mm}] = 9549 \cdot G[-] \frac{W[\text{kg}]}{N[\text{rpm}]}. \tag{1}$$

Wind turbine rotors are generally rebalanced to a residual imbalance of G16 before commissioning [11]. Guided from this classification, the levels of G32, G48 and G64 are selected as low to severe mass imbalances in operating turbines caused for example by ice accretion. The mass imbalance faults are implemented in the global simulation model by increasing the mass density of one blade by 0.58%, 0.88% and 1.17% respectively. It should be noted that ice accretion in reality also affect the aerodynamic properties of the blades, which may cause aerodynamic imbalances and reduce the electrical power output. These effects are not considered in this numerical study; the faults are rather modelled as pure inertial imbalances. The yaw misalignment cases of 5°, 10° and 15° are selected based on comparable works on yaw misalignment simulation [9,29].

The ten fault cases are simulated under six different environmental conditions (EC) adopted from Nejad et al. [28], where EC1 to EC3 are below and EC4 to EC6 are above rated wind speed of 11.4 m/s (Table 3). Each combination of FC and EC is simulated for a time period of 4000 s for 6 seeds of turbulent wind fields complying with IEC 61400-3. The numerical step size is 0.025 s for the aeroelastic simulations and 0.005 s for the drivetrain simulations. The first 400 s of simulated time series are disregarded due to simulation start-up transients and the remaining 3600 s are partitioned into 60 s sections for further signal processing. This concludes to a total number of 360 data points for each FC and EC combination.

2.2. Signal and feature selection

Synthetic SCADA and drivetrain CMS signals are generated by simulation of the aeroelastic and the drivetrain model respectively. White Gaussian noise (WGN) is added to each simulated signal to represent measurement noise. The signal-to-noise-ratio ($SNR = \sigma^2_{signal}/\sigma^2_{WGN}$) is set to a relatively conservative value of 10 based on data sheets of commercial CMS vibration sensors and typical amplitudes under normal operation. The following SCADA signals, which are traditionally used for rotor imbalance detection, are included in the analysis: rotor speed ω_{rot}, side-side nacelle accelerations $a_{Nac,Y}$ and electrical power output P_{el}. Drivetrain CMS signals are selected based on ISO 10816-21 [30], which recommends the placement of piezo-resistive or capacitive accelerometers on the housing of the main bearings, the gearbox and the generator for condition monitoring. ISO 10816-21[30] furthermore recommends the use of velocity signals by integration of measured accelerations for monitoring faults with low characteristic frequencies in the range of 0.1 to 10 Hz. The MBS drivetrain model is capable of simulating gearbox housing velocities, but is limited with regard to main bearing and generator housing vibrations, since the respective housings are not specifically implemented but rather considered part of the bedplate. The subsequent analysis focuses on gearbox housing velocities, as these represent the most realistic CMS vibration signals. The velocities are extracted in all three coordinate directions (axial v_X side-side v_Y, vertical v_Z), since ISO 10816-21[30] recommends both axial and radial measurements.

Statistical features or health indicators (HI) are generally extracted for condition monitoring, which should ideally be sensitive to faults and increase monotonically with fault progression to facilitate fault diagnosis by trend analysis [31]. According to ISO 10816-21[30], the recommended feature for general drivetrain CMS is the root mean square, however other time-domain statistical variables including mean, kurtosis, skewness, peak value, crest factor are also applied [31]. In this specific case, however, the once per revolution (1P) vibration amplitude and phase are reported to be much more effective features to detect rotor imbalance faults, and show a linear correlation with the magnitude and the location of the fault under idealized conditions [7]. The 1P-amplitude and the 1P-phase of vibration signals describe the dynamic turbine response to the imbalance loads, which are typically sinusoidal with a frequency of 1P. Discrete Fourier transform (DFT) can be applied to calculate these features, however, the variability of the rotor speed must be taken into consideration, which leads to smearing of the 1P-peak in the frequency spectrum and may introduce errors in the amplitude estimates. For this reason, computed order tracking (COT) is applied, which is commonly used in rotating machinery to eliminate the influence of shaft speed variations when extracting characteristic bearing and gear fault frequencies [32]. COT is a resampling and interpolation technique that transforms a discrete signal from the time domain to the angular domain using shaft speed measurements. The signal x measured at constant time intervals given by the sampling frequency $f_s = 1/\Delta t$ is resampled in the angular domain with equidistant angular increments $\Delta\alpha$

$$x(i\Delta t) \mapsto x^*(n\Delta\alpha). \tag{2}$$

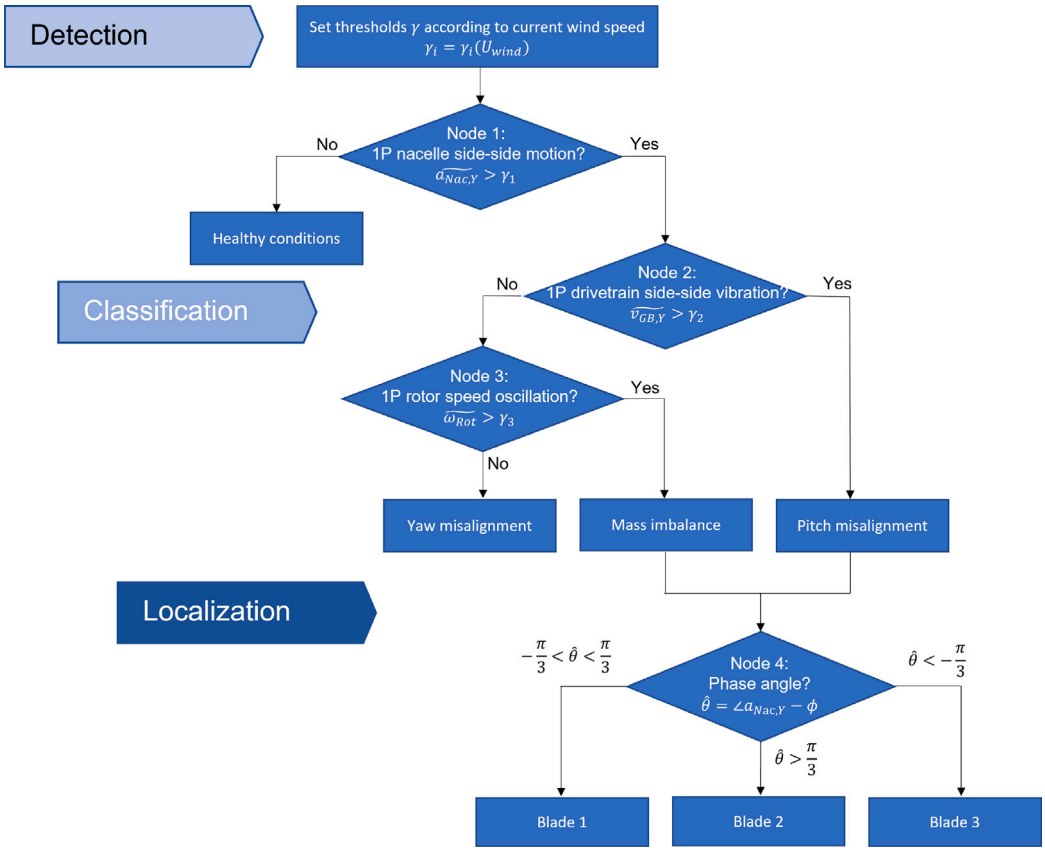

Fig. 1. Proposed knowledge-based expert system for diagnosis of rotor imbalance faults using SCADA and CMS measurements. $\widetilde{a_{Nac,Y}}$: Nacelle side-side acceleration amplitudes, $\widetilde{v_{GB,Y}}$: CMS vibration amplitudes at the gearbox housing, $\widetilde{\omega_{Rot}}$: Rotor speed amplitudes.

The 1P-amplitude $\tilde{x}$ and 1P-phase $\angle x$ are then calculated in the angular domain by DFT [33]

$$\begin{aligned} \tilde{x} &= \sqrt{\hat{a}_1^2 + \hat{a}_2^2}, \\ \angle x &= \arctan\left(\frac{-\hat{a}_2}{\hat{a}_1}\right). \end{aligned} \tag{3}$$

where

$$\begin{aligned} \hat{a}_1 &= \frac{2}{N}\sum_{n=0}^{N} x^*(n\Delta\alpha)\cdot\cos(n\Delta\alpha), \\ \hat{a}_2 &= \frac{2}{N}\sum_{n=0}^{N} x^*(n\Delta\alpha)\cdot\sin(n\Delta\alpha). \end{aligned} \tag{4}$$

The 1P-amplitude and phase are selected as statistical feature for all SCADA and CMS vibration signals that indicate the wind turbine dynamic response. For the electrical power signals the mean value is chosen, as it is reported that both pitch and yaw misalignment decrease the power production [4,21].

2.3. Proposed fault diagnosis strategy

The proposed diagnostic method for rotor imbalances comprises the three steps detection, classification and localization, as depicted in Fig. 1. Fault detection is realized with methods of statistical change detection from normal behaviour (Section 2.3.1). Classification of the rotor imbalance type uses domain knowledge formalized as an expert system (Section 2.3.2). Identification of the faulty blade is based on maximum likelihood estimates of the phase angle (Section 2.3.3).

2.3.1. Fault detection by statistical change detection

Statistical change detection is a robust methodology for fault detection under noise and unknown disturbances [22]. It provides a framework to identify statistically significant changes to the normal behaviour, which captures the naturally occurring variation of measurements from turbulence, wakes and other environmental influences. In statistical change detection the null-hypothesis H_0 and the alternative hypothesis H_1 are defined [33], representing in this case healthy and faulty behaviour. A sequence of independent random variables $x[n], n = 1, 2...N$ is sampled in order to test for each hypothesis. Under healthy conditions H_0 the samples $x[n]$ are assumed to be normally distributed with mean μ_0 and standard deviation σ_0. Under faulty conditions the dynamic response deviates from its normal behaviour, which entails a change in the distribution parameters of $x[n]$. The mean value μ_1 under H_1 is assumed to increase, while the standard deviation σ_1 is considered invariant. The assumptions of normal distributions and constant standard deviation is supported by the simulation results (Section 3.3). It is found that the signal variance is primarily a result of wind turbulence and insensitive to the fault case. The problem at hand is referred to as a binary hypothesis testing problem and expressed by Eq. (5)

$$\begin{aligned} H_0 &: x[n] \sim N(\mu_0, \sigma_0), \\ H_1 &: x[n] \sim N(\mu_1, \sigma_1),\ \mu_1 > \mu_0, \sigma_1 = \sigma_0. \end{aligned} \tag{5}$$

It is feasible that the operator has acquired knowledge of the distribution parameters under H_0, known as the normal behaviour model, from historical measurements. However, the behaviour under any rotor fault given by μ_1, σ_1 is considered unknown. In this scenario the generalized likelihood ratio test (GLRT) provides the optimal decision criterion or *test statistic*. The GLRT decides for the hypothesis H_1, if the likelihood ratio $L(x)$, given by Eq. (6), exceeds a threshold γ [33]

$$L(x) = \frac{p(x; \hat{\mu}_1,\ \hat{\sigma_1}, H_1)}{p(x; H_0)} > \gamma. \tag{6}$$

The unknown mean μ_1 is replaced by its maximum likelihood estimate (MLE) $\hat{\mu}_1$ given by the sample mean $\bar{x}$ (Eq. (7)), while the unknown

variance σ_1^2 is assumed to be identical to the variance of healthy conditions σ_0^2

$$\hat{\mu}_1 = \bar{x} = \frac{1}{N}\sum_{n=0}^{N-1} x[n], \quad \hat{\sigma}_1 = \sigma_0. \tag{7}$$

By inserting the Gaussian probability density functions and substituting the MLE (Eq. (7)) in the likelihood ratio (Eq. (6)), the test statistic $T(x)$ can be derived as the scaled square of the sample mean, as shown in Eq. (8)

$$T(x) = \frac{N\bar{x}^2}{\sigma_0^2} > \gamma'. \tag{8}$$

Under the assumption of normally distributed variables $x[n]$ (Eq. (5)), the test statistic follows a Chi-squared distribution with degrees of freedom ν and non-centrality parameter λ. With this information, adequate thresholds γ' can be set such that a maximum probability of false alarm P_{FA} is met, as shown in Eq. (9), where F^{-1} expresses the inverse cumulative density function of the non-central Chi-squared distribution

$$\gamma' = F^{-1}(1 - P_{FA}; \nu = 1, \lambda = \frac{N\mu_0^2}{\sigma_0^2}). \tag{9}$$

The probability of false alarm serves as a parameter to balance false positive and false negative rates [33]. Frequent false positives are disruptive to the wind turbine operation and detrimental to the productivity, while the missed detection of a fault (false negative) is potentially harmful and may lead to critical failures. The reported value of P_{FA} in comparable publications on statistical fault detection in wind turbines ranges widely from 10^{-2} to 10^{-12} [34,35]. In this study P_{FA} is set to 10^{-4}.

2.3.2. Knowledge-based fault classification: Expert system

Wind turbine operators may not have sufficient training data to construct data-driven models or quantitative domain knowledge to formulate accurate aeroelastic models for model-based diagnosis, but instead have acquired heuristic expertise in the form of qualitative system behaviour, conditional statements or causal relations of faults and effects. Knowledge-based methods exhibit high flexibility in data representation and thus take full advantage of such heuristic domain knowledge. In this paper, a knowledge-based expert system is proposed, which is developed with qualitative knowledge of rotor imbalance effects. For comparison, a classical data-driven approach is presented in Section 2.4 using a Linear Discriminant Analysis (LDA) classifier, which is constructed by regression on training data of faulty conditions.

Expert systems are knowledge-based methods that can find application in drivetrain condition monitoring [36,37]. Kusnick et al. [11] also presented an expert system for pitch misalignment and mass imbalance diagnosis. Expert systems are predictive models that map observations to fault types by recursive application of decision rules and thus mimic and automate human reasoning in the process of problem solving [38]. The decision rules and hierarchical structure of expert systems are formulated with the knowledge-base, a collection of domain-knowledge maintained by experienced professionals. The main advantages of expert systems are the high transparency of the decision process, which positively affects the trust of stakeholders in the diagnosis, and low requirements of quantitative domain knowledge for implementation. Limitations of expert systems are the high uncertainties in the thresholds of decision rules, which are commonly addressed with fuzzy logic or probabilistic methods.

The proposed expert system, depicted in Fig. 1, distinguishes between the four classes Healthy, Mass imbalance, Yaw misalignment and Pitch misalignment with three binary decision rules. Statistical change detection methodology is adopted to formulate the decision rules. Each node is considered a binary hypothesis testing problem, specifically a mean-shifted Gauss problem (Eq. (5)). The decision rules are then given by the test statistic in Eq. (8) and respective thresholds, which are a function of the normal behaviour model μ_0, σ_0 and the parameter P_{FA} (Eq. (9)). Since the normal behaviour is strongly influenced by environmental conditions, measurements of current wind speed U_{wind} are necessary to set appropriate thresholds. The first node represents fault detection by testing for increased side-side nacelle acceleration amplitudes $\widetilde{a_{Nac,Y}}$ caused by periodical shear forces. Both aeroelastic simulations in this study (Section 3.3) and literature suggest that $\widetilde{a_{Nac,Y}}$ is a universal indicator of any rotor imbalance type. In the second node pitch misalignment is isolated by testing for increased lateral gearbox housing vibrations at 1P ($\widetilde{v_{GB,Y}}$), which indicate periodic out-of-plane bending moments that are characteristic for pitch misalignment (Section 3.3). Lastly, mass imbalance is distinguished from yaw misalignment by its characteristic oscillation in rotor speed ($\widetilde{\omega_{Rot}}$) induced by gravitational imbalances (Section 3.3). The probability of false alarm is set to a relatively low value of $P_{FA} = 10^{-4}$ in all three nodes, which correspond to high detection thresholds γ_i.

2.3.3. Fault localization by phase angle estimation

In addition to the classification of the rotor imbalance type, it is necessary to localize the fault, i.e. identify the blade with deviating mass or pitch angle, in order to perform corrective measures. The fault location is defined as the angle θ in the rotor plane, where $\theta = 0$ refers to blade 1, $\theta = 2\pi/3$ to blade 2 and $\theta = -2\pi/3$ to blade 3. It can be derived analytically that the phase of the 1P harmonic of nacelle accelerations is directly related to the fault location in the rotor [7]. The fault location is obtained by correcting the 1P-phase estimate $\angle x$ (Eq. (3) with the current rotor azimuth angle ϕ. The rotor azimuth angle is commonly measured with encoders on the main shaft and logged in the SCADA system

$$\hat{\theta} = \angle x - \phi. \tag{10}$$

Lastly, the estimated fault location $\hat{\theta}$ is associated with the blade number using the boundaries $\pi/3$ and $-\pi/3$ (Fig. 1).

2.4. Reference fault diagnosis method: Linear discriminant analysis

A Linear Discriminant Analysis (LDA) classifier is selected as a benchmark to evaluate the proposed diagnostic method. LDA is a supervised machine learning method used for classification [39]. The prerequisites for LDA are similar to those of the statistical change detection method, in that (a) each class k follows multivariate Gaussian distributions and (b) shares a common covariance matrix $\vec{\Sigma}$, which are valid assumptions according to the simulation results (Section 3.3)

$$H_k : \vec{x} \sim N(\vec{\mu}_k, \vec{\Sigma}), \quad \vec{\Sigma}_k = \vec{\Sigma} \forall k. \tag{11}$$

LDA distinguishes between classes k, in this context fault types, by imposing a sample vector $\vec{x}$ of different predictors (here sensor signals) on linear discriminant functions δ_k. The class G is predicted, whose mean vector $\vec{\mu}_k$ is most closely aligned with the sample vector $\vec{x}$ and thus maximizes the respective linear discriminant function (Eq. (12))

$$\begin{aligned} G(\vec{x}) &= \text{argmax}_k(\delta_k) \\ &= \text{argmax}_k \left(\vec{x}^T \vec{\Sigma}^{-1} \vec{\mu}_k - \frac{1}{2}\vec{\mu}_k^T \vec{\Sigma}^{-1} \vec{\mu}_k + \ln \pi_k \right), \end{aligned} \tag{12}$$

where

$$\begin{aligned} \vec{\mu}_k &= \frac{1}{N_k}\sum_k^{N_k} \vec{x}_k, \\ \vec{\Sigma} = \vec{\Sigma}_1 &= \frac{1}{N_k - 1}\sum_k^{N_k} (\vec{x}_k - \vec{\mu}_1)(\vec{x}_k - \vec{\mu}_1)^T. \end{aligned} \tag{13}$$

The distribution parameters $\vec{\mu}_k$, $\vec{\Sigma}$ and class priors π_k are not known beforehand and must be estimated with labelled training data. The class priors of each class are identical, since an equal number of simulations are conducted for each FC, and can thus be omitted in Eq. (12). The mean vector and covariance matrix are determined by their maximum likelihood estimate (Eq. (13)).

Table 4
First principles analysis of rotor imbalances and induced drivetrain responses.

Fault type	Mass imbalance		Pitch misalignment		Yaw misalignment	
Imbalance forces	$F_G = const$ ⇓	$F_C = const$ ⇓	$\Delta F_N = const$ ⇓	$\Delta F_t = const$ ⇓	$\Delta F_N(\omega t)$ ⇓	$\Delta F_t(\omega t)$ ⇓
Rotating frame	$M_x(\omega t)$ ⇓	$F_z = const$ ⇓	$M_y = const$ ⇓	$F_y = const$ ⇓	N/A ⇓	
Fixed frame	$M_X(\omega t)$ ⇓	$F_{Y,Z}(\omega t)$ ⇓	$M_{Y,Z}(\omega t)$ ⇓	$F_{Y,Z}(\omega t)$ ⇓	$F_Y(\omega t)$ ⇓	
Structural response	–	$\ddot{Y}(t)$	–	$\ddot{Y}(t)$	$\ddot{Y}(t)$	
Drivetrain response	$\dot{\omega}(t)$	–	$\dot{Y}(t)$	–	–	

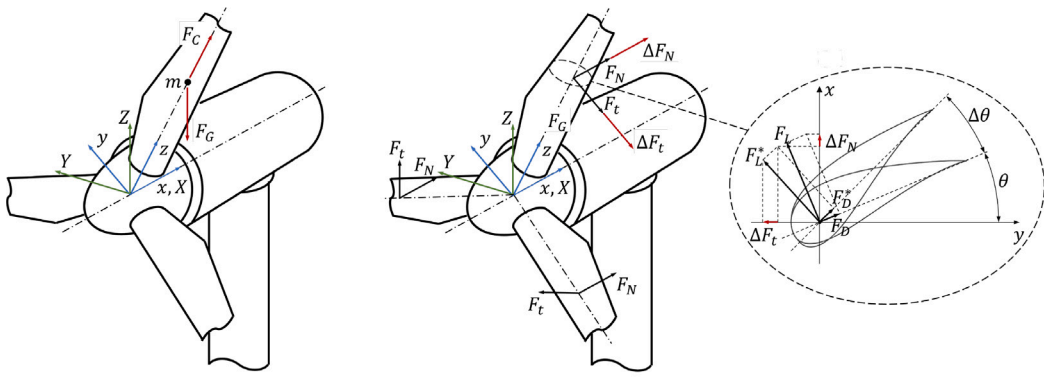

(a) Mass imbalance (b) Pitch misalignment

Fig. 2. Imbalance forces in rotating (x, y, z) and fixed coordinate frame (X, Y, Z) for different rotor imbalances.

3. Results and discussion

3.1. Analysis based on first principles

For the development of robust, physics-based diagnostic methods, it is crucial to understand the physical relationship of faults and dynamic system responses. In this section a short elaboration on the effect of rotor imbalance faults on main shaft loads in the rotating and fixed frame and their corresponding dynamic responses in the wind turbine structure and drivetrain is presented and summarized in Table 4. An idealized case without turbulence, wind shear, rotor axis tilt and tower shadow effects is considered to better isolate the primary effects of rotor imbalances.

Mass imbalance can be represented by a point mass m with distance r from the rotor axis that entails imbalance forces in the form of gravitational F_G and centrifugal forces F_C (Fig. 2). Centrifugal imbalance forces cause constant main shaft loads in the radial direction of the rotating frame (F_z), which translate to periodical shear forces in the fixed frame (F_Y, F_Z). Shear forces primarily excite transverse bending modes of the tower. Gravitational imbalance forces are constant in the fixed frame, but cause torque oscillations (M_x, M_X) due to periodical changes of lever length (ΔY), which excite torsional modes of the drivetrain.

A pitch misalignment of $\Delta\theta$ leads to discrepancies of lift forces F_L and drag forces F_D between faulty and healthy blades, which in turn can be represented as differences in thrust ΔF_N and tangential forces ΔF_t. Thrust imbalances translate to constant bending moments in the rotating frame (M_y) and periodical yaw and tilting moments in the fixed frame (M_Y, M_Z). Imbalances in tangential forces correspond to constant circumferential forces in the rotating frame (F_y) and periodical shear forces in the fixed frame (F_X, F_Y). The combination of shear forces and bending moments has an impact on both structural and drivetrain responses. Shear forces pass through the main bearings into the structure due to the high radial bearing stiffness and excite transverse tower bending modes, while out-of-plane bending moments primarily excite bending modes of the main shaft, which further impact the dynamics of downwind gear stages.

In the case of yaw misalignment, the effective angle of attack varies periodically as a function of the blade azimuth angle; it is increased in the upper half of the rotor disk and decreased in the lower half compared to non-yawed conditions. As a result the thrust and tangential forces of each blade oscillate in the rotating frame ($F_t(\omega t), F_N(\omega t)$). The load effects of yaw misalignment on the tower and the drivetrain are highly complex and can exhibit both upwards and downwards trends depending on the operational region and the yaw angle sign [29,40]. Dynamic responses to yaw misalignment are reportedly increased tower sway and platform roll motions due to shear force excitations [41].

3.2. Main shaft loads

The qualitative analysis of rotor imbalance dynamics in Section 3.1 is underlined with aeroelastic simulation results of the global wind turbine model. The analysis is limited to the amplitudes of the once per revolution (1P) oscillatory load component, where the effect imbalance faults is observable. Shown in Fig. 3 are the 1P-amplitudes of main shaft loads averaged over 6 realizations of one hour simulations for each FC–EC combination. The loads are extracted at the rotor hub in the fixed reference frame, where X is aligned with the rotor axis. First, a significant influence of environmental conditions can be observed. Shear forces (F_Y) and out-of-plane bending moments (M_Y, M_Z) show a positive trend with increasing wind speeds due to higher aerodynamic loads. Thrust (F_X) and torque (M_X) on the other hand level off or decrease above rated wind speed, which can be attributed to the pitch control system limiting the aerodynamic torque. Furthermore, there is a discernible peak in the thrust excitations at EC3 ($U = 10$ m/s), which is slightly below rated wind speed. Similar results are reported by Nejad et al. [42], where the highest axial damage equivalent loads (DEL) in floating offshore wind turbines are simulated at $U = 11$ m/s. Nejad et al. argue that the frequent activation and deactivation of the pitch control system in the region close to rated wind speed is the causes of increased axial DEL.

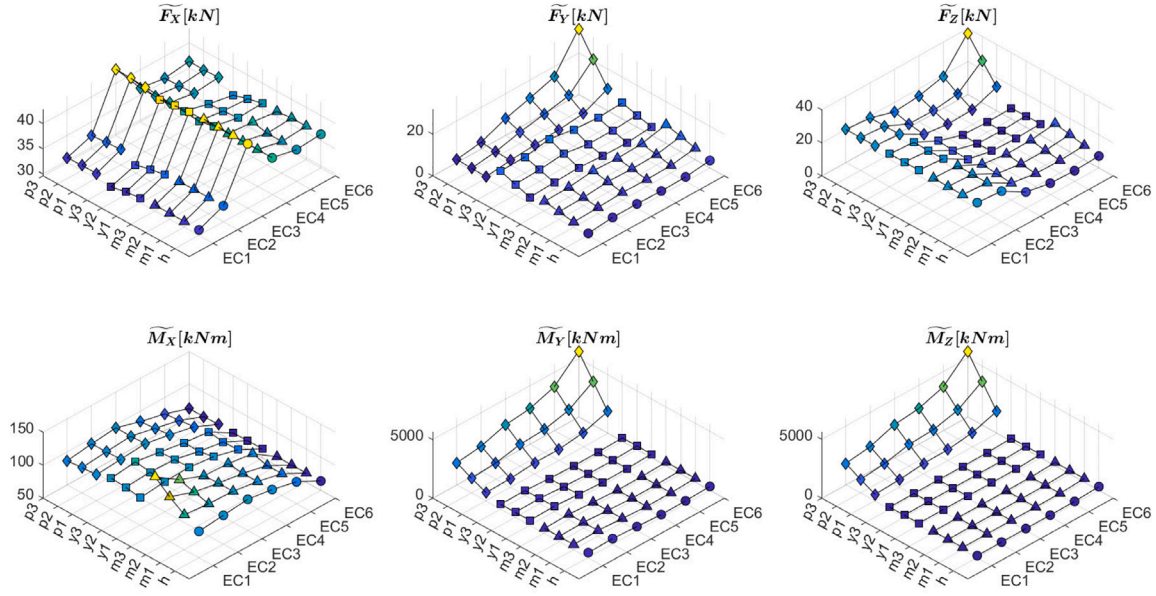

Fig. 3. 1P-amplitude $\tilde{x}$ (Eq. (3)) of main shaft loads averaged over 6 seeds of one hour simulations for different rotor imbalances and environmental conditions.

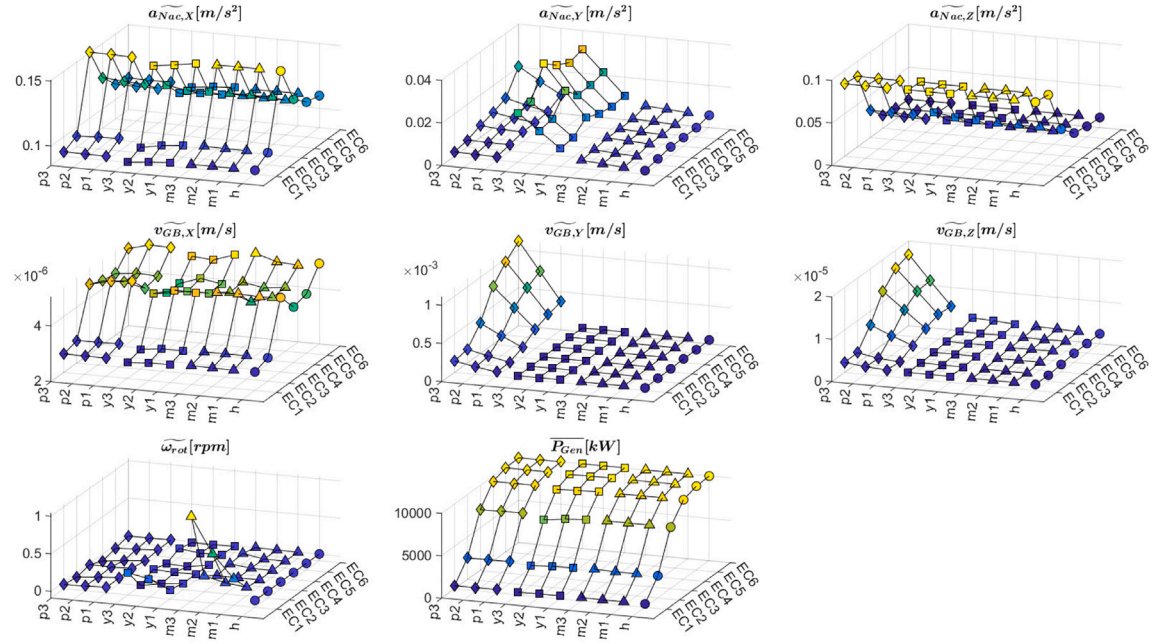

Fig. 4. 1P-amplitude (Eq. (3)) of global and drivetrain signals averaged over 6 seeds of one hour simulations of for different rotor imbalances and environmental conditions.

The effect of different rotor imbalances is indicated in Fig. 3 by the change relative to healthy conditions (h). It is apparent that mass imbalances (m1, m2, m3) cause significant excitations in shear (F_Y) and vertical forces (F_Z) due to centrifugal forces (F_C, Table 4), as well as torsional excitations (M_X) from gravitational forces (F_G, Table 4). Torsional excitations are only noticeable at lower wind speeds (EC1, EC2), where gravitational forces are more significant compared to aerodynamic forces. At EC1 the torque amplitudes due to mass imbalance reach 135 kN m, which amounts to 22% of the mean aerodynamic torque of 616 kN m. For reference, at EC6 the torque amplitudes of 55 kN m are insignificant compared to the rated aerodynamic torque of 10,000 kN m. Yaw misalignment (y1, y2, y3) appears to consistently increase amplitudes of shear forces (F_Y) for all EC, while the effect other load components is insignificant. Similar results are reported by Cardaun et al. [29]. Pitch misalignment (p1, p2, p3) results in high excitations in shear (F_Y), vertical forces (F_Z) from circumferential force imbalances (ΔF_t, Table 4) and out-of-plane bending moments (M_Y, M_Z), which can directly be attributed to thrust imbalances (ΔF_N, Table 4). In this regard pitch misalignment is unique, as it is the only rotor imbalance fault that causes 1P excitation with bending moments.

3.3. Dynamic structural and drivetrain responses

Dynamic responses in the wind turbine structure and the drivetrain to the periodic imbalance forces discussed in Section 3.2 are characterized with a selection of simulated SCADA and drivetrain CMS signals, shown in Fig. 4. Indicative of structural dynamics are nacelle accelerations a_{Nac} in fore-aft (X), side-side (Y) and vertical (Z) direction. Gearbox housing velocities v_{GB}, as well as rotor speed ω_{Rot} and electrical power output P_{el} are shown to illustrate the lateral and

torsional drivetrain response. The vibration signals at the main bearings and the generator exhibit similar behaviour to the gearbox housing signals and are omitted for brevity. The respective statistical features 1P-amplitude or mean are calculated for each signals and averaged over 6 seeds of one hour simulations for each FC–EC combination. Central to this discussion is the signal sensitivity towards faults, which is required for robust fault detection. The signal sensitivity is formally quantified by the change in mean value relative to the signal variance ($S = \frac{\mu_1 - \mu_0}{\sigma_0}$) and is indicated in Fig. 4 by the slope with respect to increasing fault severity.

Mass imbalances appear to increase side-side nacelle motion as a result of periodic shear forces, as well as increase torsional vibration in the drivetrain due to torque imbalances. Increased torsional vibrations are unique to mass imbalance faults, however the signal sensitivity is relatively low except at cut-in wind speeds (EC1). This is likely a result of the high aerodynamic torque that overshadows any torque amplitudes from mass imbalances (Section 3.2). The effect of yaw misalignment can primarily be observed in an increase of nacelle side-side acceleration amplitudes, which show a high sensitivity. The drivetrain torsional dynamics are affected by yaw misalignment as well, however a consistent upwards or downwards trend cannot be observed. Furthermore, it is evident that yaw misalignment reduces the mean electrical power by reducing the effective inflow wind speed, as stated in many references, however the environmental influences seem to dominate over effects of yaw misalignment. Unique dynamic responses to pitch misalignment can be observed in the drivetrain vibration signals that show increased velocity amplitudes in side-side and vertical direction, which are likely a result of periodic out-of-plane bending moments. In addition, pitch misalignment increases nacelle side-side motion with shear force excitation similar to the other rotor imbalance faults. A minor reduction in power output is also observed due to reduced lift forces at the faulty blade.

In conclusion, the following characteristic traits of each rotor imbalance are identified, which are leveraged as heuristic domain knowledge for the proposed diagnostic method:

- Increased side-side nacelle acceleration amplitudes as a result of periodical shear forces may be used universally for detection of any type of rotor imbalance.
- Pitch misalignment may be isolated from other fault types by increased lateral drivetrain vibration amplitudes caused by out-of-plane bending moments.
- Mass imbalance may be identified at lower wind speeds by increased rotor speed oscillations due to torque excitations.

3.4. Fault detection by means of drivetrain CMS signals

Focus of this section is to assess the capabilities of drivetrain CMS signals relative to traditionally used SCADA signals for fault detection. According to statistical change detection theory [33], the probability of detection is primarily affected by three factors: the signal sensitivity ($S = \frac{\mu_1 - \mu_0}{\sigma_0}$), the sample size N and the probability of false alarm P_{FA}. The signal sensitivity towards faults is discussed for different signals in Section 3.3. Increased sample sizes N effectively reduce the variance of the test statistic and thus improve the confidence in fault detection. Two test scenarios with sample lengths of 10 and 60 min ($N = [10, 60]$) are considered here to analyse the influence of N and to give an indication of expected detection times. The parameter P_{FA} regulates the expected false positive rate by increasing or decreasing the detection threshold. In field operation P_{FA} must be set appropriately to balance costs of false positives and detection rates. In this study a relatively low value of $P_{FA} = 10^{-4}$ is assumed.

The test statistic $T(x)$ (Eq. (8)) is applied on samples of simulated drivetrain CMS and SCADA signals in order to quantitatively assess fault detection performances. The detection thresholds (Eq. (9)) are set for each signal and EC based on training data of healthy behaviour only. The testing data set consists of 360 realizations of the statistical features mean and 1P-amplitude extracted from 1 min intervals for each FC–EC combination. The resulting true positive rates (TPR) aggregated for all environmental conditions are shown in Tables 5, 6 for sample lengths of 10 and 60 min respectively.

The electrical power signal $\overline{P_{el}}$, shows underwhelming performance with TPR of less than 10% for the severe pitch and yaw misalignment cases p3, y3. The signal sensitivity appears to be insufficient to reliably detect pitch and yaw misalignment based a one hour observation. Side-side nacelle acceleration amplitudes $\widetilde{a_{Nac,Y}}$ show a response for every rotor imbalance type. The highest TPR (> 0.95) are calculated for yaw misalignment, even for short time frames of 10 min. The signal is less sensitive to pitch misalignment and mass imbalance with maximum TPR of 0.64 and 0.61 for one hour observations. Hence, nacelle accelerations may be utilized as a universal detector for rotor imbalances, however larger sample sizes are necessary for robust detection of all fault types. Rotor speed amplitudes $\widetilde{\omega_{Rot}}$ can be used in principle for mass imbalance detection, however with a maximum TPR of 0.22 the detection performance is inferior to nacelle accelerations. Gearbox housing vibration signals show a significant response to pitch misalignment, predominantly in side-side direction $\widetilde{v_{GB,Y}}$, which results in TPR near 1 for a 10 min sample. Similar results are obtained for vibration signals at the main bearings and the generator housing, which are omitted for brevity.

It is concluded that drivetrain vibration signals are particularly beneficial for the detection of pitch errors, since they show much higher sensitivity than classical nacelle acceleration signals.

3.5. Classification performance

The proposed knowledge-based expert system and the reference LDA classifier are trained and tested on the simulated SCADA and CMS signals $\widetilde{a_{Nac,Y}}, \widetilde{v_{GB,Y}}, \widetilde{\omega_{Rot}}$ using 6-fold cross validation. The expert system is trained exclusively on data of healthy conditions to determine the normal behaviour model (μ_0, σ_0) and set the thresholds γ_i (Eq. (9)), while LDA classifier is trained on the entire dataset to estimate distribution parameters $\vec{\mu}_k, \Sigma_k$ (Eq. (13)) of each fault case. Each EC is trained and tested separately to factor out influences of wind speed, which would be available from measurements in field operation.

The results for the expert system are shown in Fig. 5 as confusion matrices. Confusion matrices relate the predicted values of a classifier with the actual values and are commonly used for performance assessment in machine learning. The diagonal elements denote the number of instances, where a class is correctly predicted, whereas the off-diagonal elements represent misclassifications between classes. The individual fault severity levels (eg. m1, m2, m3) are aggregated into a single class (m), since the method is unable to estimate these. First, it is observed that all healthy cases with one exception are correctly classified as a result of the relatively low value of $P_{FA} = 10^{-4}$ and corresponding high detection thresholds. In addition, all pitch misalignment cases are correctly identified regardless of the environmental conditions, which suggests that the gearbox housing vibration signal $\widetilde{v_{GB,Y}}$ is effective at isolating this fault type. Yaw misalignment is correctly predicted in the majority of cases using nacelle accelerations $\widetilde{a_{Nac,Y}}$ with the exception of three misclassifications as mass imbalance. Mass imbalance is identified in 10 out of 18 cases at cut-in wind speeds (EC1) using rotor speed amplitudes $\widetilde{\omega_{Rot}}$. At higher wind speeds, however, the signal sensitivity of $\widetilde{\omega_{Rot}}$ is insufficient such that mass imbalances are either not detected or misclassified as yaw misalignment. Reasons for the low sensitivity at higher wind speeds may be higher influences of the aerodynamic torque compared to the torque excitation from gravitational imbalance. It is also feasible that above rated wind speeds the pitch controller is actively damping the 1P torque fluctuations.

For comparison, the results for a traditional LDA classifier are presented in Fig. 6. The LDA classifier is able to predict both fault type and fault severity, as it is trained on a labelled dataset of faulty conditions.

Table 5
True positive rates for fault detection with a 10 min sample size ($N = 10$) with test statistic $T(x)$ (Eq. (8)).

		h	m1	m2	m3	p1	p2	p3	y1	y2	y3
Classical SCADA	$\overline{P_{el}}$	0.98	0.02	0.02	0.03	0.02	0.03	0.03	0.03	0.03	0.04
	$\widetilde{a_{Nac,Y}}$	1	0.01	0.06	0.23	0.05	0.25	0.42	0.95	1	1
	$\widetilde{\omega_{Rot}}$	0.98	0.03	0.04	0.07	0.02	0.02	0.02	0.02	0.02	0.02
Proposed drivetrain CMS	$\widetilde{v_{GB,X}}$	1	0	0	0	0	0.01	0,01	0	0	0
	$\widetilde{v_{GB,Y}}$	1	0	0	0	0.82	1	1	0	0	0
	$\widetilde{v_{GB,Z}}$	1	0	0	0	0.59	0.75	0.89	0	0	0.01

Table 6
True positive rates for fault detection with a 60 min sample size ($N = 60$) with test statistic $T(x)$ (Eq. (8)).

		h	m1	m2	m3	p1	p2	p3	y1	y2	y3
Classical SCADA	$\overline{P_{el}}$	1	0	0	0	0	0	0.03	0	0	0
	$\widetilde{a_{Nac,Y}}$	1	0.14	0.31	0.64	0.19	0.44	0.61	1	1	1
	$\widetilde{\omega_{Rot}}$	0.94	0.06	0.17	0.22	0.06	0.06	0.06	0.06	0.06	0.06
Proposed drivetrain CMS	$\widetilde{v_{GB,X}}$	1	0	0	0	0	0	0	0	0	0
	$\widetilde{v_{GB,Y}}$	1	0	0	0	1	1	1	0	0	0
	$\widetilde{v_{GB,Z}}$	1	0	0	0	0.67	0.81	1	0	0.03	0.14

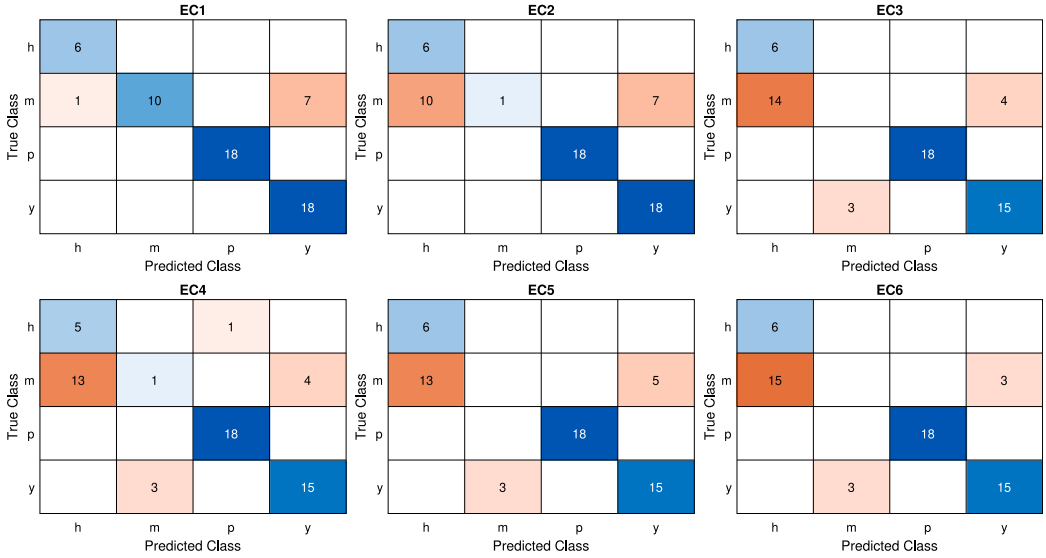

Fig. 5. Confusion matrix for knowledge-based expert system (Section 2.3.2) tested on one hour samples of simulated SCADA and CMS signals under healthy conditions (h) and rotor imbalance faults (m, p, y).

With regard to pitch misalignment and yaw misalignment classification the performance is comparable to the expert system with a TPR of close to 100%. The prediction of mass imbalance is significantly improved: Mass imbalance is longer misclassified as yaw misalignment, however it still suffers from low detection rates due to a generally weak dynamic system response and low signal sensitivities.

From these results it can be concluded that the SCADA signals $\widetilde{a_{Nac,Y}}$ and $\widetilde{\omega_{Rot}}$ in combination with the CMS signal $\widetilde{v_{GB,Y}}$ are suitable to detect and classify the three considered rotor imbalance types, at least at lower wind speeds. With the inclusion of training data of faulty conditions, the classification accuracy may be improved, however such information is rarely available in practice.

3.6. Fault localization accuracy

The accuracy of localizing the faulty blade is displayed in Fig. 7 for both classical SCADA signals and the proposed CMS drivetrain signals. The fault location is estimated with Eq. (10) based on one hour samples and shown here aggregated for all environmental conditions. In all simulated cases the fault is implemented at blade 1, which corresponds to $\theta = 0$. The results show that an accurate localization of mass imbalances is possible with the phase of nacelle acceleration signals $\angle a_{Nac,Y}$. The expected error (mean ± standard deviation) ranges from $-0.1 \pm 27.4.5°$ (m1) to $2.0 \pm 16.4°$ (m3). The remaining signals show standard errors of higher than ±100° and are thus not suitable for localizing mass imbalance. The best performance for localizing pitch misalignment show side-side gearbox housing velocities $\angle v_{GB,Y}$ with errors between $0.6 \pm 11.2°$ (p1) to $0.1 \pm 13.2°$ (p3). This is a significant improvement compared to classical SCADA signals ($\angle a_{Nac,Y}$), which result in much higher standard errors of up to ±71.5° (p1)

Similar conclusions as in Section 3.4 can be drawn in that drivetrain CMS vibration signals outperform classical SCADA signals and facilitate the detection and localization of pitch errors with much higher accuracy. For mass imbalance and yaw misalignment, however, the classical approach with nacelle acceleration signals prevails.

3.7. Considerations for field implementation and sources of uncertainty

Implementation of the proposed knowledge-based diagnostic method requires only the normal behaviour model. In practice, this

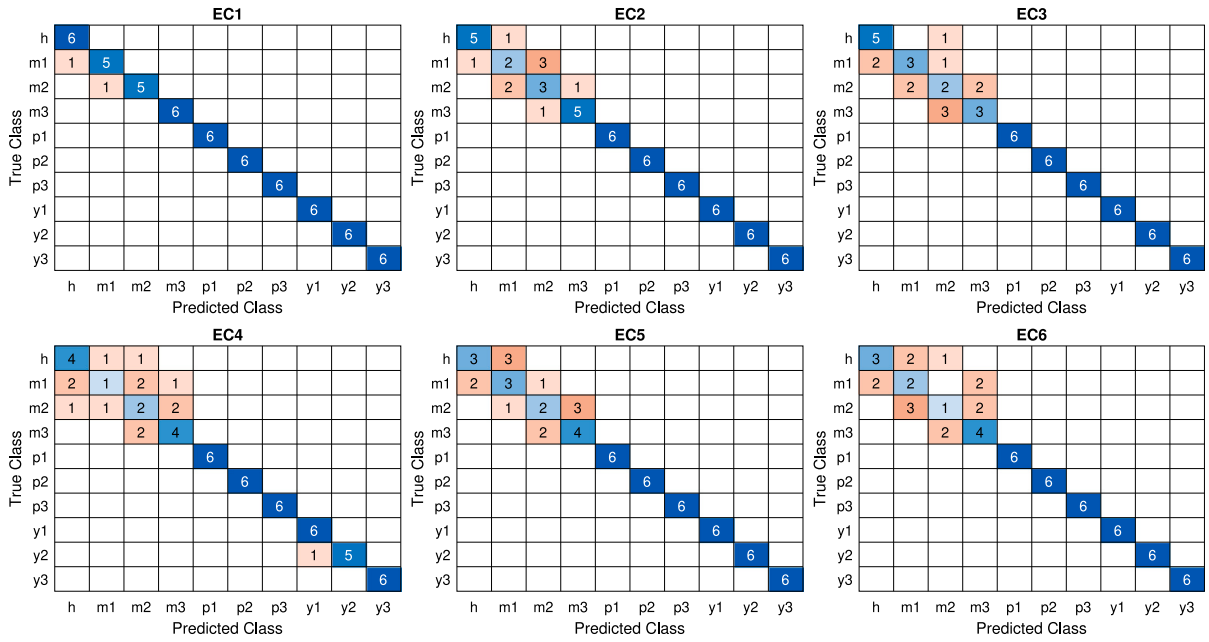

Fig. 6. Confusion matrix for data-driven LDA classifier (Section 2.4) trained and tested on one hour samples of simulated SCADA and CMS signals under healthy conditions (h) and rotor imbalance faults of varying severity (m, p, y).

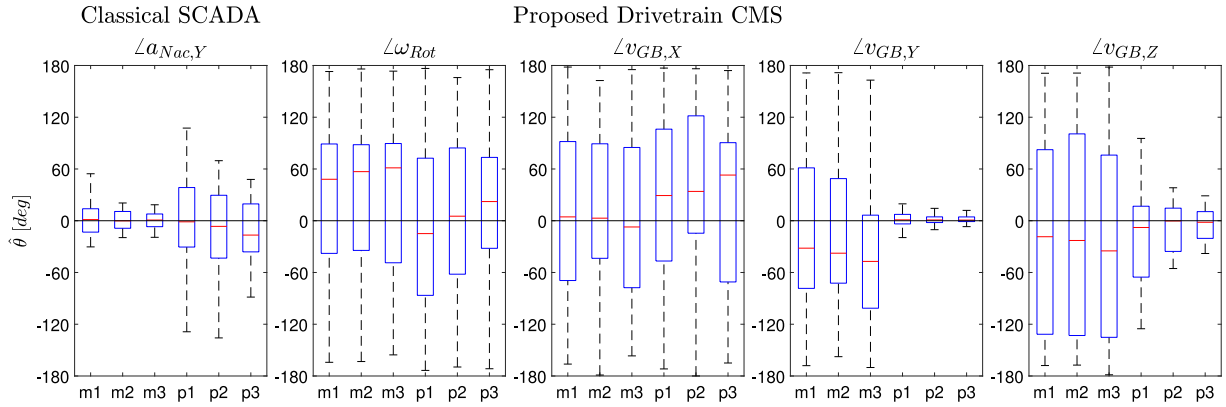

Fig. 7. Estimated fault location $\hat{\theta}$ (Eq. (10)) based on 60 min samples of simulated SCADA and CMS signals. Shown are median, 25 and 75 percentiles, and extreme values aggregated for all EC. The true fault location is $\theta = 0$ (blade 1).

would entail measuring long-term mean values and standard deviation of the signals nacelle side–side acceleration, gearbox housing side–side vibrations, and rotor speed for different wind speed bins.

It is feasible to integrate the proposed diagnostic method with resilient control techniques, which aim at minimizing fault consequences by compensating the faulty signal. Resilient control strategies for pitch misalignment are presented by Bertele et al. [7], who propose a rebalancing algorithm to iteratively correct for pitch imbalance. Other signals compensation methods such as Takagi–Sugeno fuzzy models may also be applicable in this case [43].

In addition, the detection thresholds must be set to appropriate values using the parameter P_{FA} (Eq. (9)). Unfortunately, standards or guidelines on setting detection thresholds for this specific application have not been developed yet, and the values of P_{FA} reported in scientific publications range widely from 10^{-2} to 10^{-12} [34,35]. Lower thresholds are desirable to maximize fault detection rates and to mitigate potentially harmful consequences of rotor imbalance faults such as increased fatigue loads, reduced lifetime and higher risks of failure of wind turbine components. On the other hand, low thresholds are conducive to false positives and lead to unnecessary activation of automatic rebalancing algorithms, which are disruptive to the wind turbine operation. This represents an optimization problem with the objective of minimizing the combined costs associated with false negatives K_{FN} and false positives K_{FP} and can be expressed with a cost function K [44]

$$\min_{P_{FA}} K = K_{FP} + K_{FN} \tag{14}$$

Defining the cost functions of false positives K_{FP} and false negatives K_{FN} is challenging, as it requires extensive economical analysis and risk assessment on the effects of rotor imbalance faults. Wind farm operators may instead resort to empirical methods based on confidence intervals commonly employed for drivetrain condition monitoring. Typical threshold values are $\gamma = \mu_0 + 3\sigma_0$, which corresponds to a 99.7% confidence interval [45].

Lastly, several limitations of the presented methodology and other sources of uncertainty need to be carefully considered for implementation in the field.

- *Simulation model limitations*: Simulation-based studies with academic reference models are effective for demonstrating the proof of concept of novel methods. Simulation models enable the exploration of many different fault scenarios in a short time frame,

however due to model assumptions and complexity reduction they do not fully reflect the dynamics of real wind turbines. The 10 MW DTU reference drivetrain model is considered state-of-the-art for load calculations, but is limited with regard to vibration analysis. Flexible housing models for the main bearings, gearbox and the generator are not implemented and as a result the simulated drivetrain CMS signals may suffer from inaccuracies. It should also be noted that the analysis of this paper is limited to four point support, medium speed drivetrains and that the findings are not directly transferable to direct drive systems.

- *Considered fault cases*: The scope of this paper is limited to a small amount of fault cases to retain reasonable simulation times, in particular with the computationally expensive MBS drivetrain model. Only static pitch misalignment of a single blade towards feather is investigated. Combinations of aerodynamic and mass imbalances, which are likely to occur in practice, are not considered in this study. Shaft misalignment faults are not considered in this study, but may cause similar dynamic responses at 1P and thus be misclassified as a rotor imbalance by the diagnostic method. Other faults including main bearing and gear faults are out of the scope of this paper, since they typically have much higher characteristic frequencies and would be filtered out by the proposed method.
- *Fault severity*: The proposed method is not capable of estimating the rotor imbalance severity, as this would require additional model assumptions and/or training data. For instance, the power reduction with respect to the yaw misalignment angle can be modelled with the third power of the cosine function [20]. Velocity and acceleration amplitudes can be well described by linear functions of the rotor imbalance severity, as seen in Fig. 4, however additional training data would be required to determine the unknown slopes.
- *Operational conditions*: The proposed method is only robust at cut-in wind speeds, where mass imbalance cause significant torque excitations and induce an observable torsional response in the drivetrain. At higher wind speeds the method is unable to distinguish between yaw misalignment and mass imbalance. Furthermore the method was not tested under other IEC 61400-1 load cases such as start-up or emergency shutdown.
- *Measurement noise*: Sensors in the field are subject to measurement noise and other sources of uncertainty, which could affect the diagnostic performance. However, it can be argued that the measurement noise of commercial accelerometers has relatively low energy compared to the excitations of rotor imbalance faults. Typical values for measurement noise in the low frequency range of 1P are specified to 4 μg or $4{\cdot}10^{-5}$ m/s^2 (see PCB Model 622B01), whereas simulated acceleration amplitudes under faulty conditions were of the order 10^{-4} m/s^2 at the gearbox housing and 10^{-2} m/s^2 at the nacelle (Fig. 4). Furthermore, it is observed in this study that the employed statistical methods are effective at filtering out the energetic 1P component from a noisy background.
- *Signal resolution*: Sensor data quality is also limited by the signal resolution. The minimum required sample frequency to estimate 1P-amplitudes of nacelle and drivetrain signals is 0.2 Hz at a minimum rotor speed of 6 rpm. Classical SCADA data stored as 10 min averages do not suffice for this purpose, however, it is reported that wind farm operators are moving towards high-frequency (1 Hz) SCADA data [46].

4. Conclusions

This paper presented a novel approach for diagnosis of rotor imbalance faults, namely pitch misalignment, yaw misalignment and mass imbalance, by monitoring the drivetrain vibration response. Traditionally, only SCADA signals indicative of structural dynamics including nacelle accelerations, rotor speed and electrical power are utilized for this purpose. Drivetrain CMS signals on the other hand are normally used for diagnosis of local drivetrain faults in gears and bearings. The proposed method comprises the three steps fault detection, classification and localization. Fault detection is realized with methods of statistical change detection from normal behaviour. Classification of the rotor imbalance type uses heuristic, physics-based decision criteria derived from simulations and literature review. Localization of the faulty blade is based on maximum likelihood estimates of the phase angle.

Simulations were conducted with both high-fidelity aeroelastic and drivetrain models of the floating 10 MW DTU reference turbine to synthesize SCADA and CMS signals and evaluate the proposed method. Six environmental conditions with wind speeds ranging from cut-in to cut-out and three fault severity levels were carefully selected based on literature review to emulate realistic conditions.

The proposed drivetrain CMS signal (gearbox housing side-side velocity) outperformed classical SCADA signals in detecting pitch misalignment and increased the detection rate of a 1° pitch error from 19% to near 100% based on one hour measurements. Furthermore, the standard error in localizing the blade with faulty pitch angle was reduced from 71.5° to 11.2°. For mass imbalance and yaw misalignment, however, the classical approach using nacelle accelerations remained more accurate.

The benefit of drivetrain CMS signals is also seen in the classification of the rotor imbalance type. Pitch misalignment uniquely causes once per revolution (1P) bending moments on the main shaft, which are observable throughout the drivetrain as increased lateral vibration amplitudes. Thus, the 1P-amplitudes of CMS signals are proposed as an indicator to distinguish pitch misalignment from other rotor imbalance types. Using CMS signals all simulated test cases of pitch misalignment ranging from 1° to 3° were correctly classified regardless of the environmental conditions.

A unique characteristic of mass imbalance are periodic 1P torque loads, which excite torsional modes of the drivetrain. For this reason the 1P-amplitude of the main shaft speed is proposed as an identifier for mass imbalances, however, in practice the signal sensitivity is relatively low due to environmental influences and controller effects. Only at cut-in wind speeds (EC1) this criterion was shown to be robust and able to identify 10 out of 18 of test cases. A benchmark linear discriminant analysis (LDA) classifier representative for a fully data-driven approach showed significantly higher classification performance for both mass imbalance and yaw misalignment. However, the success of this approach relies on the availability of training data of faulty conditions, which in practice is rarely the case.

From these results it can be concluded that the SCADA signals nacelle side-side acceleration ($\widetilde{a_{Nac,Y}}$) and rotor speed ($\widetilde{\omega_{Rot}}$) in combination with the CMS signal gearbox housing velocity ($\widetilde{v_{GB,Y}}$) are suitable to detect and classify the three considered rotor imbalance types, at least at lower wind speeds. For practical implementation in operating turbines it is recommended to apply the change detection framework presented in this paper, as it has very low requirements. Only the normal behaviour model of healthy conditions must be established from historical measurements. However, some method limitations have to be considered including lower accuracy than data-driven methods, the inability to estimate the fault severity, the required signal resolution of 1 Hz and the limited operational range near cut-in wind speeds.

CRediT authorship contribution statement

Felix C. Mehlan: Simulations, Data analysis, Development of methodology, Writing. **Amir R. Nejad:** Conceptualization, Review & edit, Funding.

Declaration of competing interest

The authors declare that they have no known competing financial interests or personal relationships that could have appeared to influence the work reported in this paper.

Data availability

Data will be made available on request.

Acknowledgements

The authors wish to acknowledge financial support from the Research Council of Norway through InteDiag-WTCP project (Project number 309205). The first author would also like thank Andrea Sanchez and Donatella Zappala for constructive discussions and Shuaishuai Wang for providing the 10 MW drivetrain model.

References

[1] Y. Kumar, J. Ringenberg, S.S. Depuru, V.K. Devabhaktuni, J.W. Lee, E. Nikolaidis, B. Andersen, A. Afjeh, Wind energy: Trends and enabling technologies, Renew. Sustain. Energy Rev. 53 (2016) 209–224, http://dx.doi.org/10.1016/j.rser.2015.07.200.
[2] T. Stehly, P. Beiter, 2018 Cost of Wind Energy Review, Report, National Renewable Energy Laboratory, 2020.
[3] M. Wilkinson, B. Hendriks, F. Spinato, E. Gomez, H. Bulacio, J. Roca, P. Tavner, Y. Feng, H. Long, Methodology and results of the reliawind reliability field study, in: European Wind Energy Conference, Warsaw, Poland, 2010.
[4] D. Astolfi, A study of the impact of pitch misalignment on wind turbine performance, Machines 7 (1) (2019) http://dx.doi.org/10.3390/machines7010008.
[5] U. Elosegui, I. Egana, A. Ulazia, G. Ibarra-Berastegi, Pitch angle misalignment correction based on benchmarking and laser scanner measurement in wind farms, Energies 11 (12) (2018) http://dx.doi.org/10.3390/en11123357.
[6] P. Frohboese, A. Anders, Effects of Icing on wind turbine fatigue loads, J. Phys. Conf. Ser. 75 (2007) http://dx.doi.org/10.1088/1742-6596/75/1/012061.
[7] M. Bertelè, C.L. Bottasso, S. Cacciola, Automatic detection and correction of pitch misalignment in wind turbine rotors, Wind Energy Sci. 3 (2) (2018) 791–803, http://dx.doi.org/10.5194/wes-3-791-2018.
[8] M. Saathoff, M. Rosemeier, T. Kleinselbeck, B. Rathmann, Effect of individual blade pitch angle misalignment on the remaining useful life of wind turbines, Wind Energy Sci. 6 (5) (2021) 1079–1087, http://dx.doi.org/10.5194/wes-6-1079-2021.
[9] C.L. Bottasso, C.E.D. Riboldi, Estimation of wind misalignment and vertical shear from blade loads, Renew. Energy 62 (2014) 293–302, http://dx.doi.org/10.1016/j.renene.2013.07.021.
[10] ISO 21940-11, Mechanical vibration — Rotor balancing — Part 11: Procedures and tolerances for rotors with rigid behaviour, 2016.
[11] J. Kusnick, D.E. Adams, D.T. Griffith, Wind turbine rotor imbalance detection using nacelle and blade measurements, Wind Energy 18 (2) (2015) 267–276, http://dx.doi.org/10.1002/we.1696.
[12] Z. Gao, X. Liu, An overview on fault diagnosis, prognosis and resilient control for wind turbine systems, Processes 9 (2) (2021) http://dx.doi.org/10.3390/pr9020300.
[13] R.W. Hyers, J.G. McGowan, K.L. Sullivan, J.F. Manwell, B.C. Syrett, Condition monitoring and prognosis of utility scale wind turbines, Energy Mater. 1 (3) (2013) 187–203, http://dx.doi.org/10.1179/174892406x163397.
[14] X. Gong, W. Giao, Simulation investigation of wind turbine imbalance faults, in: International Conference on Power System Technology, IEEE, 2010, http://dx.doi.org/10.1109/POWERCON.2010.5666455.
[15] G.R. Hübner, H. Pinheiro, C.E. de Souza, C.M. Franchi, L.D. da Rosa, J.P. Dias, Detection of mass imbalance in the rotor of wind turbines using support vector machine, Renew. Energy 170 (2021) 49–59, http://dx.doi.org/10.1016/j.renene.2021.01.080.
[16] J. Niebsch, R. Ronny, Simultaneous estimation of mass and aerodynamic rotor imbalances for wind turbines, J. Math. Ind. 4 (12) (2014) http://dx.doi.org/10.1186/2190-5983-4-12.
[17] S. Cacciola, I.M. Agud, C. Bottaso, Detection of rotor imbalance, including root cause, severity and location, J. Phys. Conf. Ser. 753 (2016) http://dx.doi.org/10.1088/1742-6596/753/7/072003.
[18] A. Kusiak, A. Verma, A data-driven approach for monitoring blade pitch faults in wind turbines, IEEE Trans. Sustain. Energy (2010) http://dx.doi.org/10.1109/tste.2010.2066585.
[19] S. Cho, M. Choi, Z. Gao, T. Moan, Fault detection and diagnosis of a blade pitch system in a floating wind turbine based on Kalman filters and artificial neural networks, Renew. Energy 169 (2021) 1–13, http://dx.doi.org/10.1016/j.renene.2020.12.116.
[20] D. Choi, W. Shin, K. Ko, W. Rhee, Static and dynamic Yaw misalignments of wind turbines and machine learning based correction methods using LiDAR data, IEEE Trans. Sustain. Energy 10 (2) (2019) http://dx.doi.org/10.1109/TSTE.2018.2856919.
[21] B. Jing, Z. Qian, Y. Pei, L. Zhang, T. Yang, Improving wind turbine efficiency through detection and calibration of Yaw misalignment, Renew. Energy 160 (2020) 1217–1227, http://dx.doi.org/10.1016/j.renene.2020.07.063.
[22] M. Ghane, A. Rasekhi Nejad, M. Blanke, Z. Gao, T. Moan, Condition monitoring of spar-type floating wind turbine drivetrain using statistical fault diagnosis, Wind Energy 21 (7) (2018) 575–589, http://dx.doi.org/10.1002/we.2179.
[23] C. Bak, F. Zahle, R. Bitsche, T. Kim, A. Yde, L.C. Henriksen, M.H. Hansen, J.P.A.A. Blasques, M. Gaunaa, A. Natarajan, The DTU 10-MW Reference Wind Turbine, Report, DTU Wind Energy, 2013.
[24] R.R. Arias, J. Galvan, NAUTILUS-DTU10 MW Floating Offshore Wind Turbine at Gulf of Maine, WindEurope, 2018.
[25] OpenFAST, https://github.com/OpenFAST.
[26] Dassault Systèmes, Simpack: Multibody simulation, 2021, https://www.3ds.com/fileadmin/PRODUCTS/SIMULIA/PDF/brochures/simulia-simpack-brochure.pdf.
[27] S. Wang, A.R. Nejad, T. Moan, On design, modelling, and analysis of a 10-MW medium-speed drivetrain for offshore wind turbines, Wind Energy 23 (4) (2020) 1099–1117, http://dx.doi.org/10.1002/we.2476.
[28] A.R. Nejad, E.E. Bachynski, M.I. Kvittem, C. Luan, Z. Gao, T. Moan, Stochastic dynamic load effect and fatigue damage analysis of drivetrains in land-based and TLP, spar and semi-submersible floating wind turbines, Mar. Struct. 42 (2015) 137–153, http://dx.doi.org/10.1016/j.marstruc.2015.03.006.
[29] M. Cardaun, B. Roscher, R. Schelenz, G. Jacobs, Analysis of wind-turbine main bearing loads due to constant yaw misalignments over a 20 years timespan, Energies 12 (9) (2019) http://dx.doi.org/10.3390/en12091768.
[30] ISO10816-21, Mechanical vibration — Evaluation of machine vibration by measurements on non-rotating parts — Part 21: Horizontal axis wind turbines with gearbox, 2015.
[31] R.B. Randall, Vibration Based Condition Monitoring: Industrial, Aerospace and Automotive Applications, Wiley I& Sons Ltd, 2010.
[32] K.S. Wang, P.S. Heyns, Application of computed order tracking, Vold–Kalman filtering and EMD in rotating machine vibration, Mech. Syst. Signal Process. 25 (1) (2011) 416–430, http://dx.doi.org/10.1016/j.ymssp.2010.09.003.
[33] S.M. Kay, Fundamentals of Statistical Signal Processing. Volume II. Detection Theory, Prentice Hall PTR, 1998.
[34] S. Nath, J. Wu, Y. Zhao, W. Qiao, Low latency bearing fault detection of direct-drive wind turbines using stator current, IEEE Access 8 (2020) 44163–44174, http://dx.doi.org/10.1109/access.2020.2977632.
[35] M. Ghane, A.R. Nejad, M. Blanke, Z. Gao, T. Moan, Statistical fault diagnosis of wind turbine drivetrain applied to a 5MW floating wind turbine, J. Phys. Conf. Ser. 753 (2016) http://dx.doi.org/10.1088/1742-6596/753/5/052017.
[36] W. Qiao, D. Lu, A survey on wind turbine condition monitoring and fault diagnosis—Part II: Signals and signal processing methods, IEEE Trans. Ind. Electron. 62 (10) (2015) 6546–6557, http://dx.doi.org/10.1109/tie.2015.2422394.
[37] M.C. Garcia, M.A. Sanz-Bobi, J. del Pico, SIMAP: Intelligent system for predictive maintenance, Comput. Ind. 57 (6) (2006) 552–568, http://dx.doi.org/10.1016/j.compind.2006.02.011.
[38] W. Li, H. Li, S. Gu, T. Chen, Process fault diagnosis with model- and knowledge-based approaches: Advances and opportunities, Control Eng. Pract. 105 (2020) http://dx.doi.org/10.1016/j.conengprac.2020.104637.
[39] T. Hastie, R. Tibshirani, J. Friedman, The Elements of Statistical Learning: Data Mining, Inference and Prediction, Springer, 2009, http://dx.doi.org/10.1007/b94608.
[40] R. Damiani, S. Dana, J. Annoni, P. Fleming, J. Roadman, J. van Dam, K. Dykes, Assessment of wind turbine component loads under Yaw-offset conditions, Wind Energy Sci. 3 (1) (2018) 173–189, http://dx.doi.org/10.5194/wes-3-173-2018.
[41] X. Li, C. Zhu, Z. Fan, X. Chen, J. Tan, Effects of the Yaw error and the wind-wave misalignment on the dynamic characteristics of the floating offshore wind turbine, Ocean Eng. 199 (2020) http://dx.doi.org/10.1016/j.oceaneng.2020.106960.
[42] A.R. Nejad, E.E. Bachynski, T. Moan, Effect of axial acceleration on drivetrain responses in a Spar-type floating wind turbine, J. Offshore Mech. Arct. Eng. 141 (3) (2019) http://dx.doi.org/10.1115/1.4041996.
[43] X. Liu, Z. Gao, M.Z.Q. Chen, Takagi–Sugeno fuzzy model based fault estimation and signal compensation with application to wind turbines, IEEE Trans. Ind. Electron. 64 (7) (2017) 5678–5689, http://dx.doi.org/10.1109/tie.2017.2677327.
[44] A. Youssef, C. Delpha, D. Diallo, An optimal fault detection threshold for early detection using Kullback–Leibler divergence for unknown distribution data, Signal Process. 120 (2016) 266–279, http://dx.doi.org/10.1016/j.sigpro.2015.09.008.
[45] A. Alkaya, I. Eker, Variance sensitive adaptive threshold-based PCA method for fault detection with experimental application, ISA Trans. 50 (2) (2011) 287–302, http://dx.doi.org/10.1016/j.isatra.2010.12.004, URL https://www.ncbi.nlm.nih.gov/pubmed/21251651.
[46] E. Gonzalez, B. Stephen, D. Infield, J.J. Melero, Using high-frequency SCADA data for wind turbine performance monitoring: A sensitivity study, Renew. Energy 131 (2019) 841–853, http://dx.doi.org/10.1016/j.renene.2018.07.068.